

## The PHOBOS Experiment at RHIC

Edmundo Garcia<sup>6</sup> for the PHOBOS Collaboration  
B.B. Back,<sup>1</sup> M.D. Baker,<sup>2</sup> D.S. Barton,<sup>2</sup> R.R. Betts,<sup>1,6</sup> R. Bindel,<sup>7</sup>  
A. Budzanowski,<sup>3</sup> W. Busza,<sup>4</sup> A. Carroll,<sup>2</sup> M.P. Decowski,<sup>4</sup>  
N. George,<sup>1</sup> K. Gulbrandsen,<sup>4</sup> S. Gushue,<sup>2</sup> C. Halliwell,<sup>6</sup>  
G.A. Heintzelman,<sup>2</sup> C. Henderson,<sup>4</sup> D.J. Hofman,<sup>6</sup> R. Hołyński,<sup>3</sup>  
B. Holzman,<sup>2,6</sup> E. Johnson,<sup>8</sup> J.L. Kane,<sup>4</sup> J. Katzy,<sup>4,6</sup> N. Khan,<sup>8</sup>  
W. Kucewicz,<sup>6</sup> P. Kulinich,<sup>4</sup> W.T. Lin,<sup>5</sup> S. Manly,<sup>8</sup> D. McLeod,<sup>6</sup>  
J. Michałowski,<sup>3</sup> A.C. Mignerey,<sup>7</sup> J. Mülmenstädt,<sup>4</sup> R. Nouicer,<sup>6</sup>  
A. Olszewski,<sup>2,3</sup> R. Pak,<sup>2</sup> I.C. Park,<sup>8</sup> H. Pernegger,<sup>4</sup> C. Reed,<sup>4</sup>  
L.P. Remsberg,<sup>2</sup> M. Reuter,<sup>6</sup> C. Roland,<sup>4</sup> G. Roland,<sup>4</sup>  
L. Rosenberg,<sup>4</sup> P. Sarin,<sup>4</sup> P. Sawicki,<sup>3</sup> W. Skulski,<sup>8</sup> S.G. Steadman,<sup>4</sup>  
P. Steinberg,<sup>2</sup> G.S.F. Stephans,<sup>4</sup> M. Stodulski,<sup>3</sup> A. Sukhanov,<sup>2</sup>  
J.-L. Tang,<sup>5</sup> R. Teng,<sup>8</sup> A. Trzupek,<sup>3</sup> C. Vale,<sup>4</sup>  
G.J. van Nieuwenhuizen,<sup>4</sup> R. Verdier,<sup>4</sup> B. Wadsworth,<sup>4</sup>  
F.L.H. Wolfs,<sup>8</sup> B. Wosiek,<sup>3</sup> K. Woźniak,<sup>3</sup> A.H. Wuosmaa<sup>1</sup> and  
B. Wyslouch<sup>4</sup>

<sup>1</sup> Argonne National Laboratory, Argonne, IL 60439, USA

<sup>2</sup> Brookhaven National Laboratory, Upton, NY 11973, USA

<sup>3</sup> Institute of Nuclear Physics, Kraków, Poland

<sup>4</sup> Massachusetts Institute of Technology, Cambridge, MA 02139, USA

<sup>5</sup> National Central University, Chung-Li, Taiwan

<sup>6</sup> University of Illinois at Chicago, IL 60607, USA

<sup>7</sup> University of Maryland, College Park, MD 20742, USA

<sup>8</sup> University of Rochester, Rochester, NY 14627, USA

*Received 21 November 2001*

**Abstract.** Since June 2000, the Relativistic Heavy-Ion Collider (RHIC) at Brookhaven National Laboratory has delivered the first collisions between Au nuclei at the highest center of mass energies achieved in the laboratory to date. PHOBOS is one of four experiments studying the Au+Au interactions at RHIC. In this paper we will describe the PHOBOS experiment, and discuss some of the current physics results obtained for Au+Au collisions at  $\sqrt{s_{NN}} = 56$  and 130 and 200 GeV. They include the study of the charged particle multiplicity as a function of pseudo-rapidity and centrality, and the measurements of the anti-

particles to particles ratios. The observed charged particle densities near mid-rapidity are higher than previously measured in any nuclear collisions. Also the rate of increase of the mid-rapidity particle density with energy is faster than that for nucleon—nucleon collisions at comparable beam energies. Finally, the antiparticle to particle ratios indicate the creation of a nearly baryon free zone at mid-rapidity.

*Keywords:* heavy-ion collisions, charged particle multiplicity, centrality dependence, antiparticle to particle ratio

*PACS:* 25-75.q, 25-75.Ld, 25.75.Dw

## 1. Introduction

The fundamental theory of strong interactions predicts that the Quark–Gluon Plasma (QGP) will be formed for systems at sufficiently high energy density [1]. The QGP was the state of matter that existed about 10 micro-seconds after the Big Bang. This state is a conglomerate of free quarks and gluons. The goal of the relativistic heavy-ion program over the past two decades has been to find the signatures of the formation of the QGP. From the data collected at the AGS, the SPS and so far from RHIC, it is clear that the search for the QGP will require a long and systematic effort of the entire physics community of this field.

At nearly the end of the second year of running, the four RHIC experiments have presented a vast body of physics measurements, mainly focused on the global characterization of the Au + Au reactions. For that purpose PHOBOS has proven to be ideal and provided the results crucial for understanding the physics of Au + Au collisions at the RHIC energy regime. PHOBOS detector has an essentially  $4\pi$  acceptance for measuring multiplicity and angular distributions of charged particles. In addition, a mid-rapidity magnetic spectrometer allows for momentum measurements and particle identification. A versatile and highly efficient trigger provides a low bias selection of events. In this paper the general properties of the detector performance are described, and the discussion of some of the first physics results from this experiment is presented.

## 2. The Apparatus

PHOBOS consists of several subsystems: the multiplicity and vertex array, with the broadest rapidity coverage at RHIC; a two-arm spectrometer, with the lowest transverse momentum acceptance at RHIC; the time-of-flight array; and the trigger detectors. Figure 1 is a drawing of the PHOBOS system.

The multiplicity and vertex array, as well as the spectrometer, are made of segmented silicon detectors. Details of the setup and layout of the silicon sensors can be found in Ref. [3] for the multiplicity array and in Ref. [2] for the spectrometer. The particle trajectories in the 2 T magnetic field are reconstructed using hit positions

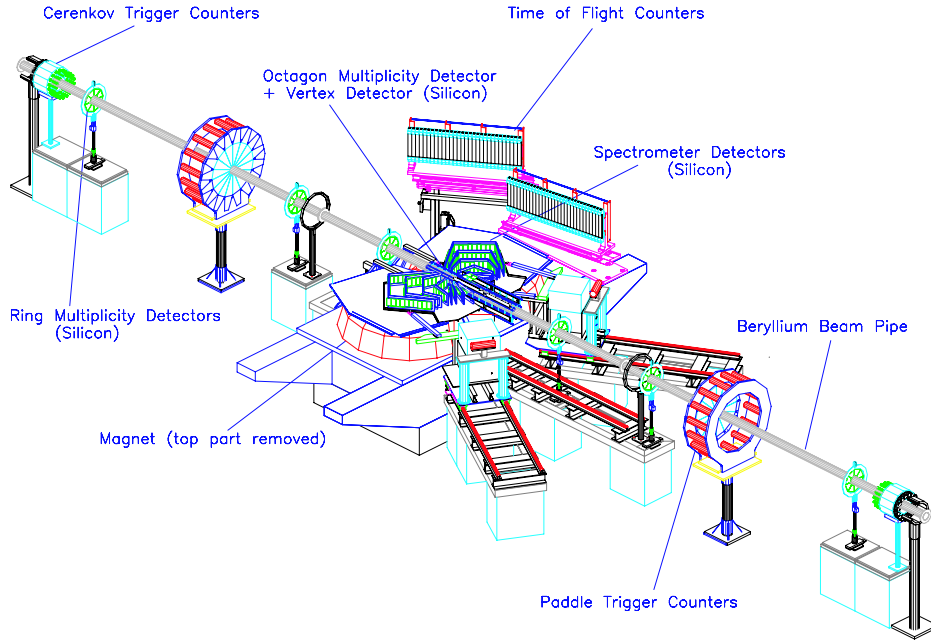


**Fig. 1.** Phobos apparatus

in the finely segmented silicon sensors. In addition, the particle identification is performed by measuring the energy deposited ( $dE/dx$ ) in the spectrometer sensors and their time of flight in the time-of-flight scintillator counters.

The multiplicity array is composed of single-layer silicon detectors providing event-by-event measurement of charged particle multiplicity for almost complete azimuthal angle coverage and for pseudo-rapidity  $|\eta| < 5.4$  (where  $\eta = -\ln(\tan(\theta/2))$ ,  $\theta$  is the polar angle from the beam axis ( $z$ )). The vertex position is measured by using hits in the two layers of silicon vertex detectors. The multiplicity detector consists of a barrel central section, the “octagon” detector, and forward ring detectors. The two-arm spectrometer covers  $0.5 \leq \eta \leq 1.5$ . Each arm of the spectrometer has a total of 16 planes of silicon sensors located on either side of the beam pipe. The spectrometer arms are placed between the poles of a magnet which provides a field of 2 T for the momentum measurements. The total acceptance of the spectrometer is about 2% of the full solid angle.

The time-of-flight array (TOF) was designed to enhance the particle identification capability of the spectrometer. It consists of two walls of 240 scintillators sitting behind the spectrometer. The system is designed to have a timing resolution of 100 ps, and will double the momentum range over which particles can be identified.

A  $\pi/K$  separation up to 0.65 GeV/c and  $p/K$  separation up to 1.2 GeV/c is expected using the spectrometer alone. Including the time of flight the separation will be extended for  $\pi/K$  up to 1.2 GeV/c and for  $p/K$  up to 1.9 GeV/c.

The trigger signals are provided by three sets of detectors: the “cerenkov” counters, the “paddle” counters and the zero degree calorimeters. The Cerenkov counters are two sets of 16 Cerenkov radiators arranged in two rings around the beam pipe covering  $4.5 < |\eta| < 4.8$ . These counters detect the occurrence of an interaction and provide a crude measure of the vertex position for the level one trigger (ready 650 ps after the interaction). The Cerenkov counters will also provide the start signal for the time-of-flight system.

The paddle counters are used as a primary minimum bias trigger or level zero trigger (ready 380 ns after the interaction). In addition they are also used to estimate the event centrality [4]. The paddle counters cover  $3.0 < |\eta| < 4.5$  and consists of the two arrays of 16 scintillators which encircle the beam line. For event triggering we use the combination of the total signal height (proportional to the number of particles), the timing information, and the number of fired scintillators.

Finally, the zero degree calorimeters (ZDCs) are also used for the level one trigger and for centrality selection. They are sampling hadron calorimeters sitting at both sides of the nominal interaction region at  $\pm 18$  m from the nominal vertex position. The ZDC measures the energy of the spectator neutrons emitted at small angles relative to the direction of the beams. The ZDC coincidence of 2 spectator neutrons is a minimal bias selection for heavy-ion collisions. This make them useful as an event trigger and a luminosity monitor. For this reason, all four RHIC experiments are equipped with these detectors [5].

### 3. Physics Measurements

So far we have analyzed the following data sets. From RHIC 2000 run, the Au + Au interactions at  $\sqrt{s_{NN}} = 56$  and 130 GeV and another sample, from 2001 run with the gold beams accelerated up to 200 AGeV.

#### 3.1. Charged-particle multiplicity measurements

In this section we present the measurement of the pseudo-rapidity density of primary charged particles in Au + Au collisions at  $\sqrt{s_{NN}} = 56, 130$  and 200 GeV, for the 6% most central collisions. The details of the detector setup, data selection and estimation of errors can be found in Refs [6–8].

These data permit a systematic analysis of the particle production mechanisms in heavy-ion collisions, providing information on the interplay between hard parton-parton processes and soft processes. Predictions of particle production at these energies obtained from different models, before RHIC data become available, varied up to a factor of two.

Figure 2 shows the energy dependence of the pseudo-rapidity density normalized per participant pair for central nucleus–nucleus collisions. The results are compared

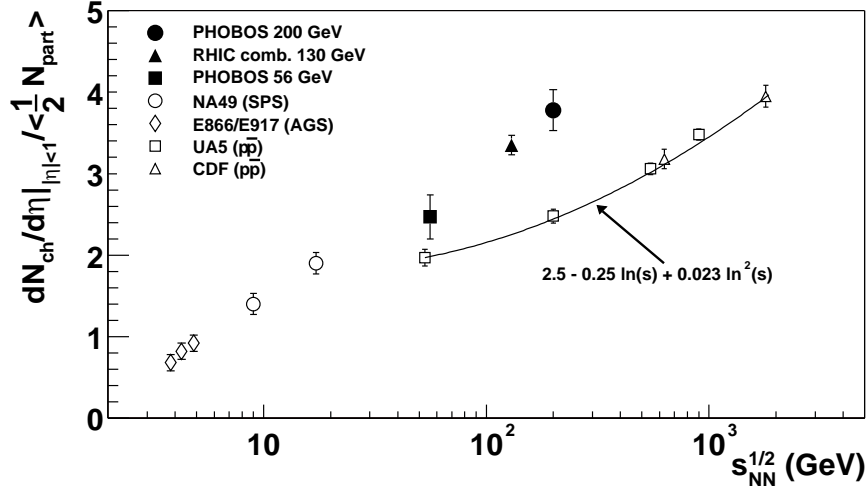
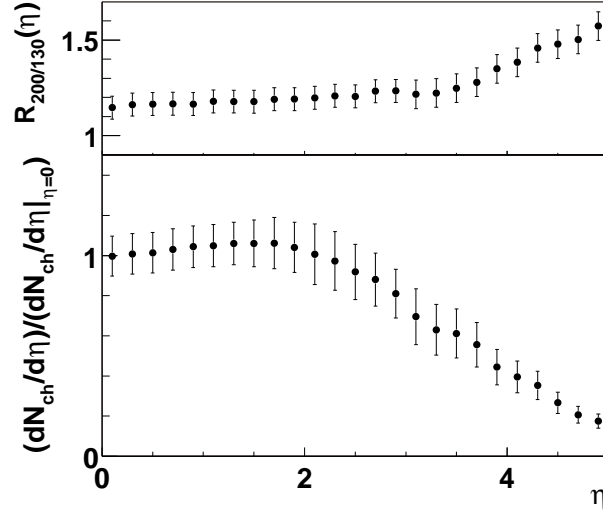


**Fig. 2.** Energy dependence of the particle pseudo-rapidity density at mid-rapidity normalized per participant pair for central nucleus–nucleus collisions. The results are compared with data from lower energies and  $p\bar{p}$  data. The solid line is a parameterization of the  $p\bar{p}$  data.

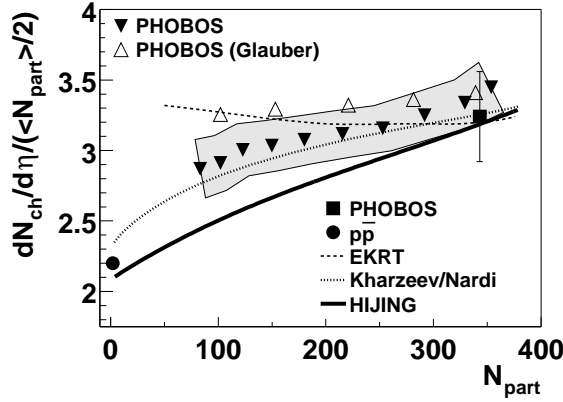
with data from lower energies and  $p\bar{p}$  data. The density at 56 GeV is  $408 \pm 12(\text{stat.}) \pm 30(\text{syst.})$ , at 130 GeV is  $555 \pm 12(\text{stat.}) \pm 35(\text{syst.})$ , and for 200 GeV was found to be  $650 \pm 35(\text{syst.})$ . The Au + Au collisions show significantly larger charged particle density per participant than the non single diffractive  $p\bar{p}$  data at comparable energies. This can be explained by a scenario that, in addition to soft processes, also includes particle production via hard-scattering processes. An increase of particle density by 31% from 56 to 130 GeV is observed, steeper than the increase expected from the parameterization of  $p\bar{p}$  data. For the energy range from 130 to 200 GeV, the increase of 14% is seen, corresponding to a moderate increase in the initial energy density in this energy interval.

Figure 3a shows the ratio of the pseudo-rapidity density at 200 GeV to the density measured at 130 GeV. A slow rise of the ratio  $R_{200/130}$  is observed up to  $\eta < 3.5$ , showing a moderate increase in particle density over the whole plateau region between the two energies. At larger  $\eta$ , a steeper rise is seen. This reflects the shift of the fragmentation region with energy. Figure 3b shows the shape of the pseudo-rapidity distribution up to  $\eta = 5$  for central collisions at 200 GeV. There is a plateau region extended up to  $\eta < 2$ , followed by a rapid drop-off toward larger pseudo-rapidities. The  $dN_{ch}/d\eta$ , normalized per participant pair, is found to be larger than in  $p\bar{p}$  collisions over the pseudo-rapidity range up to  $\eta < 4$  [7].

In Fig. 4 we compare the 130 GeV data on the measured scaled pseudo-rapidity density,  $dN_{ch}/d\eta|_{|\eta|<1}/(\frac{1}{2} <N_{\text{part}} >)$ , as a function of  $N_{\text{part}}$  (solid triangles) to several model predictions, in an attempt to discern the main mechanism for particle



**Fig. 3.** (a) Pseudo-rapidity dependence of the  $R_{200/130}$  ratio, (b) shape of  $dN_{ch}/d\eta$  at  $\sqrt{s_{NN}} = 200$  GeV



**Fig. 4.** The measured scaled pseudo-rapidity density  $dN_{ch}/d\eta|_{|\eta|<1}/(\frac{1}{2}\langle N_{part} \rangle)$  shown as a function of  $N_{part}$  (solid triangles). The error band combines the error on  $dN_{ch}/d\eta|_{|\eta|<1}$  and  $N_{part}$ . The solid circle is from  $p\bar{p}$ . The solid square is from Ref. [6]. Theoretical calculations are shown from HIJING (solid line), KN (dotted curve) and EKRT (dashed curve).

production. The details of the PHOBOS analysis of the centrality dependence of charged particle multiplicity at mid-rapidity at  $\sqrt{s_{NN}} = 130$  GeV can be found in Ref. [9].

One can see that the normalized particle density increases with increasing centrality. The results are compared to the predictions of the two-component models which assume that both, soft and hard processes contribute to particle production. Consequently, in addition to the contribution proportional to  $N_{\text{part}}$  and associated with soft processes, there is also a contribution from hard processes which scales with the number of binary nucleon–nucleon collisions. The HIJING model and the calculations of Kharzeev and Nardi (KN) follow this approach. The HIJING model (solid curve) interpolates almost linearly between the  $p\bar{p}$  point and the PHOBOS result obtained for the most central collisions. The data deviate from this prediction, and seem to follow the prediction of Kharzeev and Nardi (dotted curve). The other class of models, based on gluon saturation picture, assume that all particle production is due to hard parton–parton scattering processes. For example, the EKRT model, which incorporates a geometry dependent saturation scale, predicts a nearly constant  $dN_{ch}/d\eta/N_{\text{part}}$  as a function of  $N_{\text{part}}$ . On the other hand, the Kharzeev and Nardi model (dotted line in Fig. 4), which includes the evolution of the gluon structure functions is close to the measured data. Note, that at 130 GeV the predictions of the Kharzeev and Nardi two-component and saturation models coincide.

### 3.2. Antiparticle to particle ratios near mid-rapidity

The study of antiparticle to particle ratios in heavy-ion collisions can provide important information on the hot and dense strongly interacting matter. On a microscopic level, the  $p/\bar{p}$  ratio is sensitive to the transport of baryon number, production of quark–antiquark pairs, and the annihilation of antiprotons in the final stage of the collision. On the other hand, it has been observed at lower AGS and SPS energies that the antiparticle–particle ratios could be described via a thermodynamic description of the heavy-ion reactions, assuming chemical equilibrium. It was expected, from the extrapolation of the strongly suppressed antiproton to proton ratio observed at lower energies, that the mid rapidity region at RHIC energies would be essentially baryon free.

The ratios of antiparticles to particles for primary charged pions, kaons and protons produced at mid-rapidity were measured for the  $\sqrt{s_{NN}} = 130$  GeV data. The details of the data analysis and a discussion of systematic and statistical errors can be found in Ref. [10].

Within the detector acceptance, we find the following ratios:

$$\begin{aligned} \langle \pi^- \rangle / \langle \pi^+ \rangle &= 1.00 \pm 0.01(\text{stat.}) \pm 0.02(\text{syst.}) \\ \langle K^- \rangle / \langle K^+ \rangle &= 0.91 \pm 0.07(\text{stat.}) \pm 0.06(\text{syst.}) \\ \langle \bar{p} \rangle / \langle p \rangle &= 0.60 \pm 0.04(\text{stat.}) \pm 0.06(\text{syst.}) \end{aligned}$$

The results for  $\langle K^- \rangle / \langle K^+ \rangle$  and  $\langle \bar{p} \rangle / \langle p \rangle$  are plotted in Fig. 5 as a function of  $\sqrt{s}$ . Included in the plot are the predictions from the microscopic transport RQMD model and HIJING model, as well as the particle ratios reported at lower energies.

The  $\langle K^- \rangle / \langle K^+ \rangle$  and  $\langle \bar{p} \rangle / \langle p \rangle$  ratios measured at RHIC are significantly higher than at lower energies. Estimate of the baryo-chemical potential  $\mu_B$  within a standard statistical model with the assumed freeze-out temperature of 160–170 MeV gives  $\mu_B = 45$  MeV using the measured kaon and proton ratios. This value of  $\mu_B$  is much lower than that found from fits to the SPS data, showing a closer, but yet not complete, approach to a baryon-free regime at RHIC.

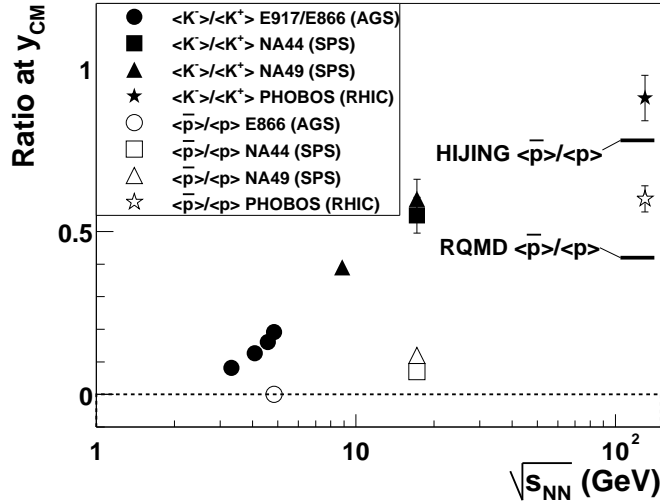


**Fig. 5.**  $\langle K^- \rangle / \langle K^+ \rangle$  and  $\langle \bar{p} \rangle / \langle p \rangle$  ratios as a function of  $\sqrt{s}$  for nucleus–nucleus collisions, in comparison with predictions from the HIJING and RQMD models. Only statistical errors are shown.

## Acknowledgments

We acknowledge the generous support of the entire RHIC project personnel, C-A and Chemistry Departments at BNL. We thank Fermilab and CERN for help in silicon detector assembly. We thank the MIT School of Science and LNS for financial support. This work was partially supported by U.S. DOE grants DE-AC02-98CH10886, DE-FG02-93ER40802, DE-FC02-94ER40818, DE-FG02-94ER40865, DE-FG02-99ER41099, W-31-109-ENG-38. NSF grants 9603486, 9722606 and 0072204. The Polish groups were partially supported by KBN grant 2 PO3B 04916. The NCU group was partially supported by NSC of Taiwan under contract NSC 89-2112-M-008-024.

## References

1. J.P. Blaizot, *Nucl. Phys.* **A661** (1999) 3.
2. H. Pernegger et al., *Nucl. Inst. Meth.* **A419** (1998) 549.
3. B. Back et al., *Nucl. Inst. Meth.* **A447** (2000) 257.
4. R. Bindel, E. Garcia, A.C. Mignerey and L.P. Remsberg, *Nucl. Inst. and Meth.* **A474** (2001) 38.
5. C. Adler, A. Denisov, E. Garcia, M. Murray, H. Strobele and S. White, *Nucl. Inst. and Meth.* **A470** (2001) 488.
6. B. Back et al. (PHOBOS Collaboration), *Phys. Rev. Lett.* **85** (2000) 3100.
7. B. Back et al. (PHOBOS Collaboration), accepted for publication in *Phys. Rev. Lett.*
8. B. Back et al. (PHOBOS Collaboration), *Phys. Rev. Lett.* **87** (2001) 102303.
9. B. Back et al. (PHOBOS Collaboration),  
<http://xxx.lanl.gov/abs/nucl-ex/0105011>.
10. B. Back et al. (PHOBOS Collaboration), *Phys. Rev. Lett.* **87** (2001) 102301.

